Theor Chem Account (2008) 119:113–131
DOI 10.1007/s00214-006-0185-2

REGULAR ARTICLE

Characterizing vibrational motion beyond internal coordinates

Werner Hug · Maxim Fedorovsky

Received: 14 February 2006 / Accepted: 31 May 2006 / Published online: 12 December 2006

Abstract We present a procedure for the decomposition of the normal modes of a composite system, including its rotations and translations, into those of fragments. The method permits—by the cross-contraction of dyads of mass-weighted displacement vectors, without recourse to valence coordinates—the direct comparison of nuclear motions of structurally similar but otherwise arbitrary fragments of molecules, and it leads to a quantitative definition of the similarity and the overlap of nuclear motions. We illustrate its usefulness by the quantification of the mixing of the normal modes of formic acid monomers upon the formation of a dimer, by the comparison of the overlap of the intermolecular normal vibrations of the water dimer computed with different ab initio schemes, and by the comparison of similarity and overlap of vibrations of (4S,7R)-galaxolide and (4S)-4-methylisochromane. The approach is expected to become a standard tool in vibrational analysis.

Keywords Overlap of nuclear motion · Similarity · Normal modes · Vibrational energy distribution

1 Introduction

The result of a molecule's normal coordinate analysis are vibrational energies and nuclear motions. Computed vibrational energies can, at least in principle, be directly likened to experimental values, though in practice anharmonicity—and the influence of the condensed phase in which the measurements are often done—limit the validity of the comparison. It is far more difficult to relate computed nuclear motions to experimental data. One way is through the calculation of vibrational absorption intensities, and of Raman scattering intensities and depolarization ratios, but for non-symmetric molecules nuclear motions are not uniquely related to these quantities [1]. For chiral molecules, two powerful tools for judging the correct rendering of vibrational nuclear motions are vibrational circular dichroism (VCD) [2–4] and Raman optical activity (ROA) [5–7]. Even with these methods, experimental confirmation of computed nuclear motions requires the agreement not just of individual bands but of patterns of bands, and of changes in patterns with changes in molecular structure, in observed and computed vibrational spectra.

The characteristic frequencies and intensities one observes in the vibrational spectra of polyatomic molecules with similar structural elements provides strong experimental evidence of the presence of similar nuclear motions in many of these molecules. Historically, the fact that empirical normal coordinate analysis was able to consistently yield vibrational motions which also show such patterns [8] therefore provided a solid argument in favor of the general qualitative correctness of computed vibrational modes. The art of rendering group vibrations, typical of small fragments of larger molecules, was honed, of course, through the use of force fields expressed in internal coordinates chosen as valence coordinates, such as the stretching of bonds, or the deformation of valence and torsional angles [9]. The approach

W. Hug (✉) · M. Fedorovsky
Department of Chemistry,
University of Fribourg, ch. du Musée 9,
Fribourg 1700, Switzerland
e-mail: werner.hug@unifr.ch

was largely unsuccessful in accounting for the differences observed in the vibrational spectra of structurally similar molecules, but it remained the only possible one in the absence of the feasibility of large quantum chemical computations.

The advent of the ab initio calculation of force fields, and the introduction of analytical gradients, has fundamentally changed the computation of molecular vibrations [10]. Force fields are now generally expressed in Cartesian derivatives rather than in valence coordinates, and off-diagonal force constants are no longer the enigmatic quantities they once were. The fact that the computation of the so-called "fingerprint" region [11,12] of the vibrational spectra of chiral molecules [13–16], and the explicit inclusion of water molecules hydrogen bonded to them [17,18], has become entirely possible is one of the best illustrations of the progress which has been achieved. The use of density functional theory (DFT), which was pioneered in vibrational optical activity for the computation of large, dissymmetric molecules [19,20], has been a key element in these developments.

The tools for interpreting the results of large calculations, on the other hand, have not kept pace with these computational developments. There have certainly been advances in the graphical representation of computed results [21], but the analysis of vibrational motions, and the correlation of data for different molecules, still either relies on the use of valence coordinates [18] or it has to be done by the visual inspection of nuclear displacements. The visual inspection can be effective [16] but it is tedious and, for large molecules, error prone as similar motions of nuclei—if the nuclei are not part of a structurally distinguished fragment—are easily missed. Valence coordinates are likewise best suited for the identification of characteristic vibrations of distinct groups of nuclei but less useful when one tries to compare vibrations in the fingerprint region. For characterizing low-frequency large-scale skeletal motions of sizable molecules, they tend to be useless.

The goal of the present work has been to develop a method which permits the decomposition of computed vibrational motions without the recourse to valence coordinates, and which allows the automatic recognition of the presence of similarity in vibrational motions of large molecules. To this end, similarity will be quantified so that it represents the extent to which the shapes of the motions of the nuclei of two vibrations resemble each other, irrespective of the relative size of the motions. This we will contrast with the notion of overlap which will be defined in such a way that it represents the fraction with which the nuclear motions of one vibration are also present in other vibrations.

2 Theory

The relevance to vibrational spectra of the results of a comparison of nuclear motions depends on how well such motions can be computed in the first place. The procedure we detail here is, by itself, mathematically strict but is subject to representing a molecule's nuclear motions by normal modes, and normal coordinates are an approximation only to the (classical) trajectories of the nuclei. The notion of normal modes supposes that a molecule's force field should be harmonic, a requirement which is never exactly satisfied.

In a normal mode, nuclei move in phase and the ratio of all coordinates is constant in time, which for non-degenerate modes implies nuclear motions along straight lines [1]. A molecule's translations and rotations satisfy the conditions for true normal modes [9,22]. They are not expressible by internal coordinates but must be included when nuclear motions in a cluster of molecules is considered. For rotations, the directions specified by normal coordinates then represent the directions of the tangents to the nuclear trajectories at the position of the nuclei in the chosen equilibrium orientation. A motion like pseudo-rotation [23], on the other hand, cannot be treated by a normal coordinate analysis, and neither can our procedure be directly applied to the comparison of such nuclear motions. To the extent that a non-rectilinear nuclear motion can be represented by a superposition of normal modes, the procedure will, however, be applicable to individual components of such a representation. An obvious example are elliptical trajectories in a doubly degenerate normal mode.

2.1 Representation of nuclear displacement vectors of one system by those of another

The transformation from the $3N$ normal modes Q_p to the $3N$ mass-weighted Cartesian displacements $q_{\alpha,i}$ of the nuclei α with mass m_α can be written as[1] [22]

$$\mathbf{q} = \mathbf{L} \cdot \mathbf{Q}, \tag{1}$$

where, in keeping with the notation as used in this article, a dot has been used to indicate a single contraction. $\mathbf{q}$ and $\mathbf{Q}$ are column vectors with the components $q_{\alpha i}$

[1] The symbol $\mathbf{L}$ is used here for the matrix which transforms normal coordinates into mass-weighted Cartesian coordinates, in keeping with earlier work [21,24]. This matrix is designated in [22] as $\mathscr{L}$, and its elements in [9,22] as l_{ik}. It should not be confused with the matrix often designated by the same symbol which connects internal and normal coordinates.

and Q_p, respectively, and

$$q_{\alpha i} = \sqrt{m_\alpha} x_{\alpha i}. \tag{2}$$

The basis in which the $x_{\alpha i}$ are expressed are the $3N$ unit vectors $\mathbf{e}_{\alpha i}$ located at the N nuclei α, with i indicating the Cartesian components.

The columns of the transformation matrix $\mathbf{L}$ are the $3N$ eigenvectors $\mathbf{L}_p$ of the Hessian matrix written in mass-weighted Cartesian coordinates. They are normalized so that

$$\mathbf{L}_p \cdot \mathbf{L}_p = \sum_{\alpha=1}^{N} \mathbf{L}_{\alpha,p} \cdot \mathbf{L}_{\alpha,p} = 1, \tag{3}$$

where the dot notation of the scalar product in Cartesian space has also been used for the eigenvectors $\mathbf{L}_p$ of a system of linear equations.[2] If one considers a single normal mode Q_p, i.e. if one assumes a single component p only of $\mathbf{Q}$ to be different from zero, then the mass-weighted displacement vector $\mathbf{q}_{\alpha,p}$ of nucleus α is given by

$$\mathbf{q}_{\alpha,p} = \mathbf{L}_{\alpha,p} Q_p. \tag{4}$$

For true vibrations, excluding translations and rotations, the actual size of the mass-weighted excursions follows from the energy of the vibration. The potential energy U_p of a vibration p is

$$2U_p = \omega_p^2 Q_p^2. \tag{5}$$

The total energy E_p of vibration p is the sum of the potential energy U_p and the kinetic energy T_p. For a harmonic oscillation the virial theorem yields $T_p = U_p$, and therefore

$$E_p = \omega_p^2 Q_p^2. \tag{6}$$

The maximum excursion corresponds to the classical turning point of motion, where all energy is in the form of potential energy. The mass-weighted maximum excursion vector $\mathbf{q}^0_{\alpha,p}$ of nucleus α therefore is

$$\mathbf{q}^0_{\alpha,p} = \frac{\mathbf{L}_{\alpha,p}\sqrt{E_p}}{\omega_p}. \tag{7}$$

E_p depends on the value of the vibrational quantum number n_p. For $n_p = 0$, i.e. for E_p equal to the zero point energy $\frac{\hbar\omega_p}{2}$, the classical mass-weighted excursion becomes

$$\mathbf{q}^0_{\alpha,p} = \mathbf{L}_{\alpha,p}\sqrt{\frac{\hbar}{2\omega_p}}. \tag{8}$$

[2] The matrices of the metric coefficients are unit matrices so that this does not lead to ambiguities, as covariance and contravariance do not need to be distinguished.

The normal modes which correspond to translations and rotations are characterized by the vanishing of a change in the potential energy, and an excursion cannot, therefore, be specified as done in Eq. (8) for vibrations. It is still entirely possible, however, to include translations and rotations in the matrix $\mathbf{L}$ of Eq. (1) because the transformation it specifies holds also for nuclear velocities. Hence, in place of (4), one can write

$$\dot{\mathbf{q}}_{\alpha,p} = \mathbf{L}_{\alpha,p} \dot{Q}_p. \tag{9}$$

Equation (9) stays physically meaningful also for translations and rotations. It is clear, however, that in comparing vectors of the $\mathbf{L}$ matrix, as we do in the following, we do not compare actual nuclear motions, even though, for the sake of simplicity, this terminology will be used where convenient. Likewise, where no confusion can arise, "mass-weighted" is not always explicitly specified where nuclear displacements are discussed.

If two systems have the same number of nuclei, then it is possible to express the vectors $\mathbf{L}_p$ of one system by those of the other, irrespective of the geometry of the systems and the masses of the nuclei. This forms the basis of our analysis of the vibrations of one system in terms of the vibrational, translational, and rotational motions of the nuclei of another. From the point of view of understanding nuclear motions, it is obvious that expressing the $\mathbf{L}_p$ vectors of one system by those of another makes sense only if there is some structural correspondence. This requires that the two systems contain groups of nuclei with a similar mass, in a geometrically similar arrangement. The nuclear motions of such similar groups of nuclei can also be compared if they are part of entities which differ in the number of their nuclei. An exact representation, however, of the nuclear motions of one system by those of the other is only possible when the compared entities themselves have the same number of nuclei.

To develop the procedure, we will use an example where the decomposition is precise. This is so for the normal modes of a dimer with $2N$ nuclei if they are expressed by the normal modes of two identical, independent monomers with N nuclei each. Apart from this choice, the treatment is general.

If we assume a non-linear geometry for the two monomers, each independent monomer has $3N - 6$ normal modes of vibration, while the dimer has $3(2N) - 6$ vibrational modes. The presence of six additional vibrational modes in the dimer, as compared to the two independent monomers, reflects the conversion into vibrations, upon the formation of a dimer, of six translational and rotational modes. In order to compare the modes of a system of two independent monomers with those of

the dimer, we first have to complement the vibrational modes of each entity by six translational and rotational normal modes. This then yields $3(2N)$ modes for the system of two independent monomers, and also for the dimer.

The vectors $\mathbf{L}_p^t$ of the translational modes can be obtained by displacing, without rotation, the center of gravity of an entity by Δx_i in three orthogonal directions i, with all distances between the nuclei being kept fixed. The components $L_{\alpha i,p}^t$ are then proportional to $\Delta x_{\alpha i}\sqrt{m_\alpha}$. The actual values of $L_{\alpha i,p}^t$ follow from the normalization condition $\mathbf{L}_p^t \cdot \mathbf{L}_p^t = 1$.

The determination of the vectors $\mathbf{L}_p^r$ of the rotational modes requires, as a first step, the calculation of the principal axes of all tensors of inertia. Each entity is then subject to a virtual rotation about each of the three principal axes. From this, one derives the directions and the ratios of the lengths of the mass-weighted displacement vectors $\mathbf{q}_{\alpha,p}^r = \Delta\mathbf{x}_{\alpha,p}^r\sqrt{m_\alpha}$. The vectors $\mathbf{L}_{\alpha,p}^r$ are proportional to these displacement vectors, and their actual length follows from $\mathbf{L}_p^r \cdot \mathbf{L}_p^r = 1$.

The vectors $\mathbf{L}_p^t$ and $\mathbf{L}_p^r$ obtained in this way are orthogonal to each other, and orthogonal to the vibrations.

2.2 Quantitative decomposition of the normal modes of a dimer

We will designate the dimer in the following with the letter A, and the two monomers of which it is composed with B and C. The unit vectors $\mathbf{e}_{\alpha i}^A$ for the displacements of the $2N$ nuclei α of the dimer form a canonical base in $\mathbb{R}^n$, with $n = 6N$:

$$\mathbf{e}_{11}^A = \begin{pmatrix} 1 \\ 0 \\ 0 \\ . \\ . \\ . \\ 0 \end{pmatrix}, \mathbf{e}_{12}^A = \begin{pmatrix} 0 \\ 1 \\ 0 \\ . \\ . \\ . \\ 0 \end{pmatrix}, \ldots, \mathbf{e}_{(2N)3}^A = \begin{pmatrix} 0 \\ 0 \\ 0 \\ . \\ . \\ . \\ 1 \end{pmatrix}. \tag{10}$$

Two indices are used in order to separately specify the number α of the nucleus and the Cartesian components i. Taken together, they represent a single index only.

If the nuclei of monomer B are numbered from 1 to N, and those of monomer C from $N+1$ to $2N$, then the combined nuclear displacements of the two monomers span the same space as the dimer. Expressed by the monomers the canonical base then is

$$\mathbf{e}_{11}^B = \begin{pmatrix} 1 \\ 0 \\ . \\ . \\ 0 \\ . \\ . \\ . \\ 0 \end{pmatrix}, \ldots, \mathbf{e}_{N3}^B = \begin{pmatrix} 0 \\ . \\ . \\ 1 \\ 0 \\ . \\ . \\ . \\ 0 \end{pmatrix};$$

$$\mathbf{e}_{(N+1)1}^C = \begin{pmatrix} 0 \\ . \\ . \\ . \\ 1 \\ 0 \\ . \\ . \\ . \\ 0 \end{pmatrix}, \ldots, \mathbf{e}_{(2N)3}^C = \begin{pmatrix} 0 \\ . \\ . \\ . \\ 0 \\ . \\ . \\ . \\ 1 \end{pmatrix}. \tag{11}$$

A vector $\mathbf{L}_p^A$ of the dimer can be written as

$$\mathbf{L}_p^A = \sum_{\alpha=1}^{2N}\sum_{i=1}^{3} L_{\alpha i,p}^A \mathbf{e}_{\alpha i}^A = \begin{pmatrix} L_{11,p}^A \\ L_{12,p}^A \\ . \\ . \\ . \\ L_{2N3,p}^A \end{pmatrix} = \begin{pmatrix} \mathbf{L}_{1,p}^A \\ \mathbf{L}_{2,p}^A \\ . \\ . \\ . \\ \mathbf{L}_{2N,p}^A \end{pmatrix}. \tag{12}$$

For the vectors $\mathbf{L}_q^B$ and $\mathbf{L}_r^C$ of the monomers B and C one has similarly

$$\mathbf{L}_q^B = \begin{pmatrix} \mathbf{L}_{1,q}^B \\ . \\ . \\ \mathbf{L}_{N,q}^B \\ 0 \\ . \\ . \\ 0 \end{pmatrix}, \quad \mathbf{L}_r^C = \begin{pmatrix} 0 \\ . \\ . \\ 0 \\ \mathbf{L}_{N+1,r}^C \\ . \\ . \\ \mathbf{L}_{2N,r}^C \end{pmatrix}. \tag{13}$$

The vectors $\mathbf{L}_p^A$ of the dimer can now be expressed by a linear combination of those of the monomers. The coefficient c_{qp}^{BA} with which $\mathbf{L}_q^B$ occurs in $\mathbf{L}_p^A$ is obtained by multiplying $\mathbf{L}_p^A$ scalar by $\mathbf{L}_q^B$

$$c_{qp}^{BA} = \mathbf{L}_q^B \cdot \mathbf{L}_p^A, \tag{14}$$

and similarly for c_{rp}^{CA}.

The signs of the coefficients c_{qp}^{BA} and c_{qp}^{CA} depend on the relative phases of $\mathbf{L}_p^A$, $\mathbf{L}_q^B$, and $\mathbf{L}_r^C$, which are arbitrary. The signs of the coefficients are therefore significant only in as much as they indicate sign changes for the combination of the monomer modes $\mathbf{L}_q^B$ and $\mathbf{L}_r^C$ in different dimer modes.

The same phase ambiguity exists when wavefunctions are compared in quantum mechanics. For wavefunctions, one has the option to compare the physically relevant densities instead. For **L**-vectors, one can compare, in an analogous fashion, dyads of vectors instead of the **L**-vectors themselves. Dyads retain the information of the relative phase of the displacement of nuclei within a normal mode (by which we mean an in-phase or out-of-phase coupling of group vibrations; motion as such is always in-phase in a normal mode). As quadratic expressions, however, dyads do not contain absolute phase information. Thus, instead of considering the coefficients c_{qp}^{BA} we can define a coefficient d_{qp}^{BA} by the double cross-contraction of the dyads of the dimer with those of the monomers

$$d_{qp}^{BA} = \mathbf{L}_q^B \mathbf{L}_q^B : \mathbf{L}_p^A \mathbf{L}_p^A. \tag{15}$$

The way in which c_{qp}^{BA} and d_{qp}^{BA} are related follows from the defining relation [25] of the double contraction[3]

$$\mathbf{L}_s \mathbf{L}_t : \mathbf{L}_u \mathbf{L}_v = (\mathbf{L}_s \cdot \mathbf{L}_u)(\mathbf{L}_t \cdot \mathbf{L}_v) \tag{16}$$

so that

$$d_{qp}^{BA} = \left(c_{qp}^{BA}\right)^2.$$

d_{qp}^{BA} therefore represents the fraction with which mode q of monomer B occurs in mode p of dimer A, and the dyads of the dimer can be written as sums of the dyads of the two monomers

$$\mathbf{L}_p^A \mathbf{L}_p^A = \sum_{q=1}^{3N} d_{qp}^{BA} \mathbf{L}_q^B \mathbf{L}_q^B + \sum_{r=1}^{3N} d_{rp}^{CA} \mathbf{L}_r^C \mathbf{L}_r^C. \tag{17}$$

The modes of two non-interacting identical monomers occur in degenerate pairs. For a dimer with appropriate symmetry, where the nuclei of the two monomers occupy equivalent sites, the modes $\mathbf{L}_q^B$ and $\mathbf{L}_{q'}^C$ of such pairs occur with the same weight in a dimer mode. It is then advantageous to form an in-phase and an out-of-phase combination of the monomer modes of a pair, and to represent the modes of the dimer in this new basis. The two linear combinations

$$\mathbf{L}_{qq'}^{BC+} = \frac{1}{\sqrt{2}}\left(\mathbf{L}_q^B + \mathbf{L}_{q'}^C\right), \quad \mathbf{L}_{qq'}^{BC-} = \frac{1}{\sqrt{2}}\left(\mathbf{L}_q^B - \mathbf{L}_{q'}^C\right), \tag{18}$$

give rise to the two dyads

$$\mathbf{L}_{qq'}^{BC\pm} \mathbf{L}_{qq'}^{BC\pm} = \frac{1}{2}\left(\mathbf{L}_q^B \mathbf{L}_q^B + \mathbf{L}_{q'}^C \mathbf{L}_{q'}^C \pm \mathbf{L}_q^B \mathbf{L}_{q'}^C \pm \mathbf{L}_{q'}^C \mathbf{L}_q^B\right). \tag{19}$$

The individual dyads which occur in the brackets have the form

$$\mathbf{L}_q^B \mathbf{L}_q^B = \begin{pmatrix} \mathbf{L}_q^B \mathbf{L}_q^B & 0 \\ 0 & 0 \end{pmatrix} \tag{20}$$

$$\mathbf{L}_{q'}^C \mathbf{L}_{q'}^C = \begin{pmatrix} 0 & 0 \\ 0 & \mathbf{L}_{q'}^C \mathbf{L}_{q'}^C \end{pmatrix} \tag{21}$$

$$\mathbf{L}_q^B \mathbf{L}_{q'}^C = \begin{pmatrix} 0 & \mathbf{L}_q^B \mathbf{L}_{q'}^C \\ 0 & 0 \end{pmatrix} \tag{22}$$

$$\mathbf{L}_{q'}^C \mathbf{L}_q^B = \begin{pmatrix} 0 & 0 \\ \mathbf{L}_{q'}^C \mathbf{L}_q^B & 0 \end{pmatrix}. \tag{23}$$

A situation which is often encountered is that two modes of a dimer, lets say $\mathbf{L}_p^{A+}$ and $\mathbf{L}_{p'}^{A-}$, can be represented to good approximation by the in-phase and out-of-phase combination of only two monomer modes. One can then write

$$\mathbf{L}_p^{A+} \approx \frac{1}{\sqrt{2}}\left(\mathbf{L}_q^B + \mathbf{L}_{q'}^C\right) \tag{24}$$

$$\mathbf{L}_{p'}^{A-} \approx \frac{1}{\sqrt{2}}\left(\mathbf{L}_q^B - \mathbf{L}_{q'}^C\right). \tag{25}$$

Double-contracting the dyads $\mathbf{L}_p^{A+}\mathbf{L}_p^{A+}$ and $\mathbf{L}_{p'}^{A-}\mathbf{L}_{p'}^{A-}$ with $\mathbf{L}_{qq'}^{BC+}\mathbf{L}_{qq'}^{BC+}$ and $\mathbf{L}_{qq'}^{BC-}\mathbf{L}_{qq'}^{BC-}$ allows us to directly identify the in-phase and the out-of-phase dimer mode, without a graphical inspection of the modes or the comparison of the relative signs of the coefficients c_{qp}^{BA} and c_{qp}^{CA}, as one has

$$\mathbf{L}_{qq'}^{BC+}\mathbf{L}_{qq'}^{BC+} : \mathbf{L}_p^{A+}\mathbf{L}_p^{A+} \approx 1 \tag{26}$$

$$\mathbf{L}_{qq'}^{BC+}\mathbf{L}_{qq'}^{BC+} : \mathbf{L}_{p'}^{A-}\mathbf{L}_{p'}^{A-} = 0 \tag{27}$$

$$\mathbf{L}_{qq'}^{BC-}\mathbf{L}_{qq'}^{BC-} : \mathbf{L}_p^{A+}\mathbf{L}_p^{A+} = 0 \tag{28}$$

$$\mathbf{L}_{qq'}^{BC-}\mathbf{L}_{qq'}^{BC-} : \mathbf{L}_{p'}^{A-}\mathbf{L}_{p'}^{A-} \approx 1. \tag{29}$$

These relations follow from the form of the dyads and the identity (16).

In the more general case, where several modes of each monomer contribute to a dimer mode, the procedure yields the fractional content with which in-phase and out-of-phase combinations occur. Only dyads transforming according to the irreducible representation of the analyzed dimer mode occur in its decomposition, which simplifies the inspection of computer-generated tables. This convenience should not be underestimated

[3] This is not the only convention for defining summation over indices in double contractions specified by a double dot, see e.g. [26]; the convention as used here is consistent with the one we used earlier [21]. Standard tensor notation avoids such ambiguities but would be far more cumbersome in the present context.

as it can be cumbersome to keep track of the relative signs of numbers in large matrices.

The procedure can be extended to dimers which lack appropriate symmetry, but in this case, the separation of the plus and minus combinations of the monomer modes in the dimer modes will be approximate only.

2.3 Overlap and similarity

We define as the overlap $O_{p'p}$ of mode p' with mode p the double contraction of the dyads of their **L**-vectors:

$$O_{p'p} = \mathbf{L}_{p'}\mathbf{L}_{p'} : \mathbf{L}_p\mathbf{L}_p. \tag{30}$$

This definition of overlap has the virtue of being independent of an arbitrary phase factor with which the **L**-vectors as solutions of a system of homogeneous linear equations can always be multiplied. If mode p' and mode p are identical, then $O_{p'p} = 1$, and for orthogonal modes, $O_{p'p} = 0$.

It is convenient to distinguish three situations:

- The modes are located on the same molecule. Their dyads are therefore orthonormal, but the notion of overlap can be applied to parts of dyads. This permits the comparison of the motion of the nuclei of a fragment for different modes.
- The modes are located on different molecules which have common structural elements. The comparison is done for the motion of the nuclei of structurally similar fragments.
- The modes of a molecule are compared with a library of standardized nuclear displacements.

The aspects which must be considered are how translational and rotational motion is taken into account, the lack of orthonormality of parts only of dyads, and the geometrical alignment of molecules, or of their fragments, which is required for the comparison of modes.

Modes located on the same molecule. If nuclear motion is compared for a fragment F, for two different modes p and p' of the same molecule, then the displacements of the nuclei of the fragment can either be compared directly, or one can compare those components only which correspond to local vibrations. In the latter case, the translations and rotations of the whole fragment need to be subtracted as shown below. Neither of the two ways is the precise equivalent of the comparison of displacements in internal coordinates, but when there is substantial motion of the whole fragment, the second way comes closer.

The direct comparison is equivalent to the double contraction of the dyads $\mathbf{L}_p^F\mathbf{L}_p^F$ and $\mathbf{L}_{p'}^F\mathbf{L}_{p'}^F$

$$O_{p'p}^F = \mathbf{L}_{p'}^F\mathbf{L}_{p'}^F : \mathbf{L}_p^F\mathbf{L}_p^F. \tag{31}$$

The separate comparison of only the vibrational components requires the determination of the translational and rotational dyads $\mathbf{L}_q^{tF}\mathbf{L}_q^{tF}$ and $\mathbf{L}_q^{rF}\mathbf{L}_q^{rF}$ of the fragment F. They can be obtained as described in the preceding section for a dimer and its monomers. The translational and rotational content of the dyad $\mathbf{L}_p^F\mathbf{L}_p^F$ follows from double-contracting it with the dyads for translations and rotations, and the vibrational component $\mathbf{L}_p^{vF}\mathbf{L}_p^{vF}$ is obtained as the difference

$$\begin{aligned}\mathbf{L}_p^{vF}\mathbf{L}_p^{vF} = \mathbf{L}_p^F\mathbf{L}_p^F &- \left(\sum_q \mathbf{L}_q^{tF}\mathbf{L}_q^{tF} : \mathbf{L}_p^F\mathbf{L}_p^F\right)\mathbf{L}_q^{tF}\mathbf{L}_q^{tF} \\ &- \left(\sum_q \mathbf{L}_q^{rF}\mathbf{L}_q^{rF} : \mathbf{L}_p^F\mathbf{L}_p^F\right)\mathbf{L}_q^{rF}\mathbf{L}_q^{rF}.\end{aligned} \tag{32}$$

For the overlap of the vibrational components of the modes p' and p on the fragment F one then has

$$O_{p'p}^{vF} = \mathbf{L}_{p'}^{vF}\mathbf{L}_{p'}^{vF} : \mathbf{L}_p^{vF}\mathbf{L}_p^{vF}. \tag{33}$$

In view of the orthogonality of vibrations, translations, and rotations, it suffices to remove the translational and rotational contaminants from one of the two contracted dyads only in Eq. (33).

The local vibrational motions obtained by removing translations and rotations are not actual vibrations of the isolated fragment, but of the fragment as part of the remainder of the molecule. In terms of the preceding discussion of the decomposition of the modes of a dimer, the local vibrational motions would correspond not to those of an independent monomer, but to those of a monomer as part of the dimer.

The analytical power of separating motions by contracting dyads transpires from looking at a simple fragment F, where F consists of just two nuclei joined by a bond. We will consider two molecular vibrational modes p and p', one representing the in-phase and the other the out-of-phase coupling of the stretching of the bond F with a similar stretching motion of another bond. The Eckart–Sayvetz conditions [22] are not, in general, satisfied for fragment F in either composite vibration. The contractions $\mathbf{L}_q^{tF}\mathbf{L}_q^{tF} : \mathbf{L}_p^F\mathbf{L}_p^F$ and $\mathbf{L}_q^{rF}\mathbf{L}_q^{rF} : \mathbf{L}_p^F\mathbf{L}_p^F$ then provide us with a quantitative measure of the contamination, by translations and rotations, of the local motions of fragment F in molecular mode p, i.e. by how much the bond F shifts and rotates. $O_{p'p}^{vF}$, and the similarly definable quantities $O_{p'p}^{tF}$ and $O_{p'p}^{rF}$, in turn measure to

which extent, for the in-phase and the out-of-phase composite vibrations p and p', the vibrational, translational, and rotational motions of the nuclei of the fragment F overlap.

Overlap only identifies a common component but it does not tell us how similar the motions of the nuclei of a fragment actually are because the compared parts of the dyads are not normalized. This can be altered by dividing the overlap by the norms of the contracted dyads:

$$S^F_{p'p} = \frac{O^F_{p'p}}{|\mathbf{L}^F_{p'}\mathbf{L}^F_{p'}||\mathbf{L}^F_{p}\mathbf{L}^F_{p}|} = \frac{\mathbf{L}^F_{p'}\mathbf{L}^F_{p'}:\mathbf{L}^F_{p}\mathbf{L}^F_{p}}{\sqrt{\mathbf{L}^F_{p'}\mathbf{L}^F_{p'}:\mathbf{L}^F_{p'}\mathbf{L}^F_{p'}}\sqrt{\mathbf{L}^F_{p}\mathbf{L}^F_{p}:\mathbf{L}^F_{p}\mathbf{L}^F_{p}}}. \quad (34)$$

$S^F_{p'p}$ measures the similarity of the *shape* of the nuclear displacements on fragment F in the molecular vibrations p' and p, independently of the actual size of nuclear excursion. The vibrational similarity $S^{vF}_{p'p}$ is defined analogously, with $\mathbf{L}^{vF}_{p}$ and $\mathbf{L}^{vF}_{p'}$ replacing $\mathbf{L}^{F}_{p}$ and $\mathbf{L}^{F}_{p'}$.

In the case of degenerate modes, no modification is necessary for overlap—the contributions of individual components of a degenerate set can simply be added. For similarity, the numerator and denominator of Eq. (34) are obtained by adding the contributions of individual components first.

Modes located on different molecules. The comparison of nuclear displacements of the nuclei of fragments of different molecules requires a directional alignment of the fragments. For small groups, e.g. two carbonyl groups, this step poses no problem. Likewise, for planar fragments with a sufficiently similar though not necessarily identical structure, like the three-nuclei OCO of a carboxylic group and the three-nuclei OCN of a primary amide group, the approximate alignment and the comparison of the displacement vectors by inspection appears manageable. The way in which the hydrogen atom attached to the oxygen, and the two hydrogen atoms attached to the nitrogen atom, can also be included in an analysis depends on the molecular vibrations one is interested in. For a low-frequency mode, the hydrogens can be combined with the O and the N atom into pseudo-atoms, and the displacements of the centers of gravity can be compared. For the OH and NH stretching vibrations, this is not a valid approach, and one would have to align the OH bond of the carboxyl group with either of the two NH bonds of the amide group.

This simple example shows that the choice of the groups of nuclei to be considered, and the way they have to be aligned, can depend on the vibration one is interested in.

A frequent situation in vibrational optical activity is the need to compare the vibrations of different molecules with the same general structure, but with a different substitution pattern. The vibrations of interest leading to the VCD and ROA signals revealing the absolute configuration of a compound often are large-scale motions which encompass much of a chiral molecule's non-planar structure [16]. The fragments to be considered then are the molecules' non-planar backbones, or large parts of them. The alignment of such fragments with a similar, but not necessarily precisely identical geometry, is thus crucial for a valid comparison of most vibrations of interest in vibrational optical activity. It cannot be done by inspection, and it will be discussed in more detail in a subsequent section.

Examples for a possible choice of fragments in the case of a sizable molecule are given in Sect. 3.3.

Comparison with a library of standardized mass-weighted nuclear displacements. The nuclear displacements of a fragment F_A of a molecule A, taken together for all normal modes of the molecule A, including translations and rotations, permit the representation of the nuclear displacements of any fragment F_B of another molecule B of different size, provided that F_A and F_B comprise the same number of nuclei. This is so even though, on a fragment only, the nuclear displacements of molecular modes are linearly dependent and do not form an orthonormal set. We can therefore write for the part $\mathbf{L}^{F_B}_q\mathbf{L}^{F_B}_q$ of the molecular dyad $\mathbf{L}^{B}_q\mathbf{L}^{B}_q$ on fragment F_B

$$\mathbf{L}^{F_B}_q\mathbf{L}^{F_B}_q = \sum_{p=1}^{3N_A} d^{F_AF_B}_{pq}\mathbf{L}^{F_A}_p\mathbf{L}^{F_A}_p, \quad (35)$$

where N_A is the number of nuclei of molecule A, F_A has the same number of nuclei as F_B, and the coefficients $d^{F_AF_B}_{pq}$ are obtained by double-contracting the local parts of dyads.

A practically useful application is the representation of the local nuclear motions of a fragment of a complex molecule by the normal modes of an identical fragment of a much smaller molecule. An example would be the exact representation of the motions of the C and the O nucleus of a carbonyl group of a large molecule by the motions of the C and the O nucleus in the normal modes of formaldehyde.

Instead of an exact representation, one is often interested in identifying that part of the nuclear motion of a large molecule which corresponds to a characteristic vibrational motion of the nuclei of a smaller one. In our simple example, this would obviously be the pure CO-stretching motion of formaldehyde. A standardized

carbonyl vibrational stretching motion can be obtained from the appropriate formaldehyde mode by removing the small translational component which the combined motion of the C and the O nucleus will have in formaldehyde. In addition, one will want to renormalize the reference dyad $\mathbf{L}^{\mathrm{ref}}_{\mathrm{CO}}\mathbf{L}^{\mathrm{ref}}_{\mathrm{CO}}$

$$\mathbf{L}^{\mathrm{ref}}_{\mathrm{CO}}\mathbf{L}^{\mathrm{ref}}_{\mathrm{CO}} = \frac{\mathbf{L}^{v}_{\mathrm{CO}}\mathbf{L}^{v}_{\mathrm{CO}}}{|\mathbf{L}^{v}_{\mathrm{CO}}\mathbf{L}^{v}_{\mathrm{CO}}|}. \tag{36}$$

The overlap $O^{vF}_{p'p}$ of a large molecule's vibrations with this standardized carbonyl-stretching motion then follows from Eq. (33), and the similarity $S^{vF}_{p'p}$ with Eq. (34).

It is possible to build a library of standardized mass-weighted nuclear displacements representative of characteristic local vibrational motions. Such a library will permit the systematic search of the vibrations of large molecules for predefined patterns of local motions.

2.4 Orientational alignment

While the representation of the normal modes of one system by those of another only requires an identical number of nuclei, the meaningful comparison of vibrational motions by Eqs. (26)–(34) also requires an orientational alignment. The geometry, even if similar, of topologically identical groups of nuclei in different molecules is, however, almost never precisely the same. In the dimer of formic acid, e.g., which will be discussed in the following section, the structure of the monomers is distorted by the formation of hydrogen bonds. An exact superposition of the positions of all nuclei is not possible in such cases, and for systems comprising more than two or three nuclei a strategy for aligning groups of nuclei must be adopted.

The problem of aligning molecules with a slightly differing geometry was first formulated in terms of rotation matrices [27,28] and later quaternions [29,30]. Quaternions, invented in the nineteenth century by the Irish mathematician W.R. Hamilton, were considered somewhat musty mathematics, less than three decades ago [25]. They have recently found renewed favor as a convenient means for the efficient rotation of objects in space, notably in the context of virtual reality.

A point in space with the position vector $\mathbf{b} = b_x\mathbf{i} + b_y\mathbf{j} + b_z\mathbf{k}$ can be represented by the quaternion $b = (0,\mathbf{b}) = 0 + b_x i + b_y j + b_z k$, where i,j,k satisfy the identities

$$i^2 = j^2 = k^2 = ijk = -1. \tag{37}$$

The relations (37) define ordinary (non-commutative but associative) quaternion multiplication. The rotation of $\mathbf{b}$ through an angle φ about a unit vector $\mathbf{n}$ through the origin can be written as the conjugation of the quaternion b with the quaternion q of unit norm,

$$b' = qbq^{-1}, \tag{38}$$

$$q = \big(\cos(\varphi/2),\ \sin(\varphi/2)\mathbf{n}\big), \tag{39}$$

$$q^{-1} = q^* = \big(\cos(\varphi/2),\ -\sin(\varphi/2)\mathbf{n}\big). \tag{40}$$

Two groups A and B can be defined by the position vectors of their N nuclei, $A = \{\mathbf{a}_\alpha\}$ and $B = \{\mathbf{b}_\alpha\}$. If B is the group to be aligned with A, then, according to Euler's theorem [25], if the two groups have an identical geometry, a rotation of B about a single suitably chosen axis is sufficient to orient it in the same way as A. After a translation of the rotated group B' into A one will have $\mathbf{b}'_\alpha = \mathbf{a}_\alpha$ for all values of α. If the geometries of A and B are not identical, a least-square criterion for minimizing the distances between equivalent nuclei can be used to define the best superposition, i.e. one can make the least square deviation

$$\varepsilon = \sum_{\alpha=1}^{N} w_\alpha \left(\mathbf{b}'_\alpha - \mathbf{a}_\alpha\right)^2 \tag{41}$$

as small as possible.

In Eq. (41), w_α are individual positive weighting coefficients one might want to attribute to different kinds of nuclei. Throughout the present work, relative atomic weights were chosen for this purpose. If chosen different from 1, the geometrical centers of A and B are defined by

$$\mathbf{r}_{\mathrm{center}} = \frac{\sum_{\alpha=1}^{N} w_\alpha \mathbf{r}_\alpha}{\sum_{\alpha=1}^{N} w_\alpha}, \tag{42}$$

where $\mathbf{r}$ stands for $\mathbf{a}$ or $\mathbf{b}$. In practice, for determining the rotation axis $\mathbf{n}$ and the rotation angle φ, the geometrical centers of A and B are first translated into the origin and the rotation of B is executed afterwards, rather then in the sequence described for explaining the principle.

The procedure for finding the quaternion q with unit norm which renders ε minimal has been described somewhat imprecisely in [29], and in more useful form in [30]. A program QTRFIT written in C is freely available [29]. In order to facilitate the use of the method in the context of the program PyVib2 [31] developed for the present work, and in order to correct an error in the coding of Eq. (42) in QTRFIT which leads to slightly erroneous results, the method was recoded in Python.

3 Computational examples

As pointed out in the theoretical section, normal coordinates describe nuclear motions by the tangents to the classical nuclear trajectories at equilibrium position. The successful computation of vibrational spectra—Raman, ROA, absorption, and VCD—by using them proves that this is not, in general, an important limitation.

Excursions, and deviations of nuclear motions from a straight line, can become substantial for localized nuclear motions, or for the motions of entities in a shallow potential. This latter case applies to some of the low-frequency motions of the hydrogen-bonded dimers discussed in Sects. 3.1 and 3.2. The reliable computation of the low-frequency part of vibrational spectra might become difficult in these cases, but tangents to nuclear trajectories can still be compared with our procedure. Our choice of relatively rigid monomers, namely H_2O and formic acid, assures, furthermore, that the comparison of the normal modes of the dimers with those of the monomers remains meaningful, with negligible mixing of monomer vibrations with large-amplitude global rotational and translational motions.

The main effect of a possible inclusion of anharmonicity is expected to be a shift of the computed frequencies towards lower values. For the H_2O dimer discussed in Sect. 3.2, the goal is the comparison of different harmonic force fields via the normal modes they entail. Anharmonicity is therefore of no concern in this case.

3.1 Mixing of modes in the formic acid dimer

In this C_{2h}-symmetric dimer, the monomers occupy equivalent sites. The covalent intramolecular bonds lead to larger force constants than do the hydrogen bonds, and many vibrations of the dimer therefore are expected to resemble, on the monomer fragments, those of the independent monomers. As the monomers do not have low energy vibrations, the six additional vibrations of the dimer should be those of lowest energy and have a pronounced intermolecular character.

Intramolecular vibrations. We denote as intramolecular those vibrations of the dimer which are expressible as linear combinations of true monomer vibrations. The vibrations 7–24 are expected to belong into this category. The procedure to analyze them is as described in Sect. 2.2, Eqs. (24)–(29), by double-contracting the dyads of the dimer vibrations with the dyads resulting from the in-phase and out-of-phase combinations of monomer vibrations.

The computations were done with the B97-1 functional [32,33] and the recent pc-2 basis set [34–36] with the Gaussian program [37]. This combination was chosen as the result of an extended study on the usefulness of DFT calculations for the computation of hydrogen bonding [38].

The numerical results in Table 1 confirm that the dimer vibrations 7–24 can almost quantitatively be represented by true monomer vibrations—the numbers in most columns add up to close to 1. It is equally evident, however, that the formation of a dimer can mix different vibrations on the same monomer, so that Eqs. (26) and (29) are not always satisfied. This is true for the 1,400–1,480 cm^{-1} wavenumber range, for the four monomer vibrations 5, 6, 5′, and 6′, which yield the four dimer vibrations 15, 16, 17, and 18. These vibrations are in-plane, mostly valence-angle bending motions involving all four hydrogen nuclei of the dimer.

In Fig. 1 we depict vibration 15 of the formic acid dimer. A decomposition of the nuclear motions into valence coordinates would be of little help for understanding its origin. Table 1, in contrast, tells us that vibration 15 of the dimer represents a mixture of 60% of the out-of-phase combination of the 2 monomer vibrations 5 and 5′, and of 40% of 6 and 6′.

The representation of the vibrations as used in Fig. 1 is in terms of vibrational energy, with the volume of the spheres chosen proportional to the fraction individual nuclei contribute to the total energy of a vibration [39]. The ratio of the kinetic energy of nucleus α in vibration p to the vibration's total kinetic energy is given by

$$\frac{T_{\alpha,p}}{T_p} = \mathbf{L}_{\alpha,p} \cdot \mathbf{L}_{\alpha,p}. \tag{43}$$

For a harmonic potential, the kinetic energy and the potential energy are equal so that Eq. (43) is also equal to the ratio $E_{\alpha,p}/E_p$ of their sum. The product $\mathbf{L}_{\alpha,p} \cdot \mathbf{L}_{\alpha,p}$ thus equaling the fractional contribution nucleus α makes to a vibration's energy. The direction of motion of the nuclei is indicated by shading. The shaded spheres must not be construed as conveying an impression of actual nuclear motion in a representation of the distribution of vibrational energy.

Other vibrations of the dimer are almost pure combinations of a single vibration of each of the two independent monomers, with Eqs. (26) and (29) well satisfied. This is true of the vibrations 19 and 20 of the CO-stretch type. Less expected is the absence of mixing for the CH-stretch vibrations 21 and 22, and the OH-stretch vibrations 23 and 24, because they are energetically close in the dimer. The mixing remains low as a consequence of local geometry and not of energetic separation. It would be larger if the OH and the CH bonds would lie on a single axis.

Table 1 Overlap of the formic acid dimer vibrations 7–24 with the in-phase (upper half) and out-of-phase (lower half) linear combinations of monomer vibrations, according to Eq. (18)

		689	721	978	1,000	1,078	1,100	1,259	1,262	1,402	1,404	1,449	1,478	1,709	1,781	3,058	3,063	3,104	3,125
		7	**8**	**9**	**10**	**11**	**12**	**13**	**14**	**15**	**16**	**17**	**18**	**19**	**20**	**21**	**22**	**23**	**24**
630	**1**	0.978	0	0	0	0	0	0.003	0	0	0	0	0.011	0	0	0	0	0	0
682	**2**	0	0	0	0.755	0	0.213	0	0	0	0	0	0	0	0	0	0	0	0
1,053	**3**	0	0	0	0.223	0	0.777	0	0	0	0	0	0	0	0	0	0	0	0
1,129	**4**	0.006	0	0	0	0	0	0.958	0	0	0	0	0.023	0.009	0	0	0	0	0
1,304	**5**	0.010	0	0	0	0	0	0.022	0	0	0.319	0	0.631	0.009	0	0	0	0.005	0
1,403	**6**	0	0	0	0	0	0	0.009	0	0	0.676	0	0.309	0.005	0	0	0	0	0
1,824	**7**	0	0	0	0	0	0	0.006	0	0	0	0	0.017	0.969	0	0	0	0.007	0
3,048	**8**	0	0	0	0	0	0	0	0	0	0	0	0	0	0	0	0.973	0.026	0
3,762	**9**	0	0	0	0	0	0	0	0	0	0.002	0	0.005	0.005	0	0	0.026	0.960	0
630	**1**	0	0.964	0	0	0	0	0	0.009	0.007	0	0.019	0	0	0	0	0	0	0.001
682	**2**	0	0	0.874	0	0.044	0	0	0	0	0	0	0	0	0	0	0	0	0
1,053	**3**	0	0	0.049	0	0.951	0	0	0	0	0	0	0	0	0	0	0	0	0
1,129	**4**	0	0.013	0	0	0	0	0	0.960	0	0	0.013	0	0	0.012	0	0	0	0.002
1,304	**5**	0	0.021	0	0	0	0	0	0.007	0.579	0	0.387	0	0	0.005	0	0	0	0.002
1,403	**6**	0	0.002	0	0	0	0	0	0.010	0.403	0	0.579	0	0	0.005	0	0	0	0
1,824	**7**	0	0	0	0	0	0	0	0.011	0.009	0	0	0	0	0.978	0	0	0	0
3,048	**8**	0	0	0	0	0	0	0	0	0	0	0	0	0	0	0.973	0	0	0.026
3,762	**9**	0	0	0	0	0	0	0	0.002	0	0	0.002	0	0	0	0.025	0	0	0.969

The criterion for in-phase and out-of-phase is the transformation property with respect to rotation about the C_2 axis. 0 stands for values below 1 part in 1,000. The small difference to 1 in each column is made up by translational and rotational monomer modes. Wavenumbers are indicated at the top and at the left. Computational approach: B97-1/pc-2

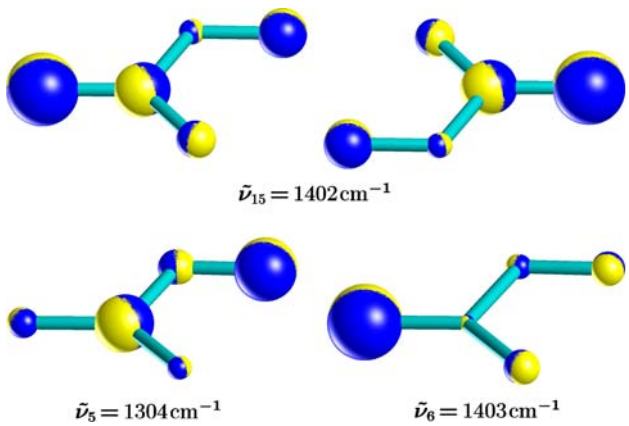

Fig. 1 Vibrational energy distribution of vibration 15 of the dimer (*top*), with the underlying monomer vibrations 5 and 6 (*bottom*) which contribute 60 and 40%, respectively. Computational approach: B97-1/pc-2

Intermolecular vibrations. The decomposition of the six vibrations of lowest energy of the dimer into the nuclear motions of the monomers, shown in Table 2, proves that they can all be represented by almost pure combinations of translational and rotational monomer modes. Rotational modes contribute far more than the translational ones. This can be understood from the Eckart–Sayvetz conditions [22]. They preclude combinations of translational motions which lead to a translation of the center of mass of the dimer. An in-phase and an out-of-phase combination of two translational monomer modes can therefore not both lead to dimer vibrations. In contrast, some monomer rotations can combine in both ways because a net angular momentum, which one of the two combinations produces, can be readily compensated for by the translational motions of the individual monomers' centers of mass. This is an important mechanism leading to the mixing of translational and rotational modes.

The dimer vibrations 3 and 5 in Table 2 are examples of such nuclear motions mainly composed of an in-phase and out-of-phase combination of the same rotational monomer modes. Vibration 6, which is shown graphically in Fig. 2, represents a 99.9% pure out-of-phase combination of rotations about the monomer axes of inertia I_3(B) and I_3(C), which are parallel to the C_2 axis of the dimer (see Fig. 3). The in-phase combination, in turn, makes an important contribution to dimer vibration 2, with translations compensating the resulting net rotation.

In addition to the vibrational energy representation, Fig. 2 also displays the shape of vibration 6 in the form of non-mass-weighted $\mathbf{L}^x$-vectors. This gives, in contrast to the energy representation, the correct impression of the rigid rotational motion of the individual formic acid

Table 2 Overlap of the in-phase combinations (upper half) and the out-of-phase combinations (lower half), according to Eq. (18), of the translational (**T**) and rotational (**R**) modes of the two formic acid monomers with the six vibrations of lowest energy of the dimer

		76	171	184	208	260	275
		1	**2**	**3**	**4**	**5**	**6**
0	$\mathbf{T}_x$	0	0.248	0	0.069	0	0
0	$\mathbf{T}_y$	0	0.210	0	0.787	0	0
0	$\mathbf{T}_z$	0	0	0	0	0	0
0	$\mathbf{R}_1$	0.007	0	0.964	0	0	0
0	$\mathbf{R}_2$	0.991	0	0.005	0	0	0
0	$\mathbf{R}_3$	0	0.533	0	0.141	0	0
0	$\mathbf{T}_x$	0	0	0	0	0	0
0	$\mathbf{T}_y$	0	0	0	0	0	0
0	$\mathbf{T}_z$	0	0	0	0	0.053	0
0	$\mathbf{R}_1$	0	0	0	0	0.850	0
0	$\mathbf{R}_2$	0	0	0	0	0.015	0
0	$\mathbf{R}_3$	0	0	0	0	0	0.999

In-phase and out-of-phase are defined as for Table 1. The small difference to 1 in each column is made up of true monomer vibrations. The numbers on the top and on the left are the frequencies of the normal modes. Computational approach: B97-1/pc-2

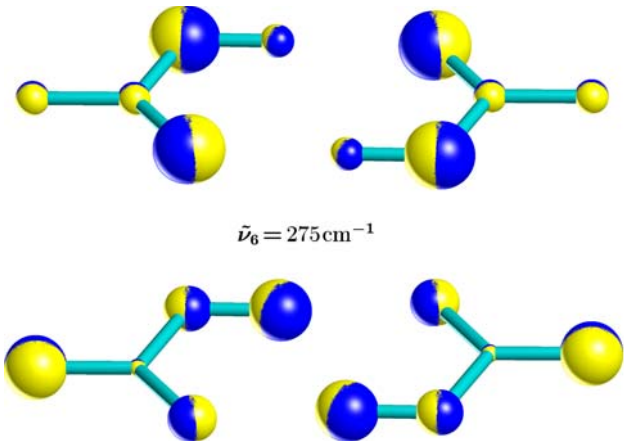

Fig. 2 Dimer mode described by the out-of-phase combination of the two rotational monomer modes about the main axes $I_3(B)$ and $I_3(C)$ of their tensors of inertia, which are parallel to the dimer's C_2 axis. *Top* vibrational energy distribution. *Bottom* nuclear displacements $\mathbf{L}^x$. Computational approach: B97-1/pc-2

units. To represent the $\mathbf{L}^x$-vectors, spheres located on nuclei are used with the spheres' diameter proportional to the size of the nuclear excursions, and with the direction of motion indicated by shading [21].

3.2 Intermolecular potential of the H_2O dimer

In the dimer, the H_2O monomers do not occupy equivalent sites. For some nuclear motions of the monomers, like, e.g., the scissoring modes, it is possible to identify an in-phase and an out-of-phase combination, but for other kinds of motions, such as the antisymmetric stretching modes, this is not meaningfully possible. Table 3 therefore lists the results of the double contractions of the dimer dyads with the dyads of the two monomers, without the previous formation of in- and out-of-phase combinations. The computations were done with the DFT B97-1/pc-2 combination already used for formic acid.

The lowest six vibrations of the dimer are pure intermolecular modes with negligible contributions from monomer vibrations. Their vibrational energy distribution is depicted in Fig. 4. Most of the true vibrational modes of the individual monomers also mix little upon dimer formation, even though the dimer's C_s symmetry only precludes the antisymmetric stretching mode 3 of monomer *B* from doing so. Two monomer vibrations which do mix are the symmetric and the antisymmetric stretching mode 2 and 3 of monomer *C*.

The compared DFT methods are B97-1/pc-2, B97-1/rr-pc-2 (see following section), B97-1/pc-1, and the O3LYP functional [40,41] combined with pc-2. The reference method is the coupled cluster approach at the CCSD(T) level with the aug-cc-pVTZ basis set [42]. The CCSD(T) calculations were done with ACESII [43]. The choice of the first two DFT methods is obvious as they are the ones used in this work. B97-1/pc-1 and O3LYP/pc-2 were included to demonstrate the importance of the choice of the basis set and of the functional.

The overlap of the mass-weighted vibrational dyads is represented by circular discs drawn with a surface proportional to overlap, with the diameter of the circles equal to the squares which contain them when overlap equals 1. Each column in the schematics given below corresponds to the decomposition of a vibration computed by a DFT method into the vibrations computed by the reference method.

All comparisons are made for harmonic force fields as it is not the purpose of the present work to consider anharmonic corrections. It its therefore not expected that

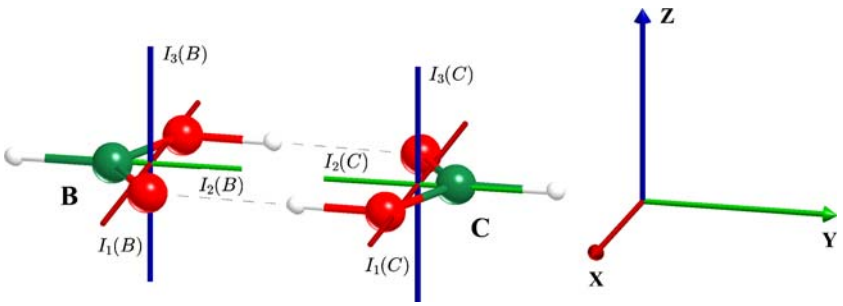

Fig. 3 Coordinate system used for the dimer A and orientation of the main axes of the two monomers' tensors of inertia designated as $I_1(B)$, $I_1(C)$, $I_2(B)$, etc. I_1 has the smallest and I_3 the largest value. The y-axis points from the center of mass of monomer B to the center of mass of monomer C, the C_2 axis is perpendicular to the (x, y)-plane, as is I_3

Table 3 Overlap of the vibrations of the water dimer A with the modes of monomer B (upper half) and of monomer C (lower half). R_1, R_2, and R_3 are rotations about the three main axes I_1, I_2, and I_3 of the individual monomers' tensors of inertia

		134	147	154	188	361	627	1,632	1,654	3,731	3,838	3,917	3,940
		1	**2**	**3**	**4**	**5**	**6**	**7**	**8**	**9**	**10**	**11**	**12**
0	$\mathbf{T}_x$	0.001	0.002	0	0	0	0.011	0	0	0	0	0	0
0	$\mathbf{T}_y$	0	0	0.160	0.340	0	0	0	0	0	0	0	0
0	$\mathbf{T}_z$	0	0	0	0	0.015	0	0	0	0	0	0	0
0	$\mathbf{R}_1$	0	0	0.455	0.221	0.315	0	0	0	0	0	0	0
0	$\mathbf{R}_2$	0.269	0.442	0	0	0	0.093	0	0	0	0	0	0
0	$\mathbf{R}_3$	0.110	0.334	0	0	0	0.066	0	0	0	0	0	0
1,632	**1**	0	0	0	0	0	0	0.957	0.043	0	0	0	0
3,844	**2**	0	0	0	0	0	0	0	0	0.005	0.994	0	0
3,948	**3**	0	0	0	0	0	0	0	0	0	0	0	1.000
0	$\mathbf{T}_x$	0.001	0.002	0	0	0	0.011	0	0	0	0	0	0
0	$\mathbf{T}_y$	0	0	0.160	0.340	0	0	0	0	0	0	0	0
0	$\mathbf{T}_z$	0	0	0	0	0.015	0	0	0	0	0	0	0
0	$\mathbf{R}_1$	0.371	0.013	0	0	0	0.420	0	0	0	0	0	0
0	$\mathbf{R}_2$	0.249	0.207	0	0	0	0.398	0	0	0	0	0	0
0	$\mathbf{R}_3$	0	0	0.226	0.098	0.650	0	0	0.004	0	0	0	0
1,632	**1**	0	0	0	0	0.004	0	0.043	0.952	0	0	0	0
3,844	**2**	0	0	0a	0	0	0	0	0	0.750	0.006	0.244	0
3,948	**3**	0	0	0	0	0	0	0	0	0.244	0	0.756	0
		1.000	1.000	1.000	1.000	1.000	1.000	1.000	1.000	1.000	1.000	1.000	1.000

I_3 (largest) is perpendicular to the plane HOH, I_2 (medium) coincides with the C_2 axis. For the directions of the translations **T** and the labeling of the monomers, see Fig. 4. Computational approach: B97-1/pc-2

computed frequencies would compare well with experimental ones, if these were known. It is equally clear, however, that agreement within the harmonic approximation is indispensable for obtaining, in a further step, the right answer for the right reason, by the explicit consideration of anharmonicity.

Figure 5 shows that agreement of the intermolecular vibrations is good for B97-1/pc-2 and CCSD(T)/aug-cc-pVTZ. A small amount of mixing of the two lowest vibrations of A'' symmetry of the reference method occurs in B97-1/pc-2. Results, not shown, for MP2/aug-cc-pVTZ and MP2/aug-cc-pVQZ calculations are similar [38].

Replacing the pc-2 set by the rr-pc-2 set (right-hand side of Fig. 5) does not substantially alter the picture. Less mixing is observed for the two lowest vibrations, and a bit more for vibrations 3, 4, and 5. It is interesting to note that augmenting either of these triple-zeta sets by diffuse functions does not produce a qualitative difference.

The situation changes when the double-zeta pc-1 set is used instead. From Fig. 6 it is evident that, while the basic shape of individual vibrations remains roughly intact, the energetic sequence does not. As the same experience is made with other double-zeta sets, we conclude that a triple-zeta set is a minimum requirement for the correct reproduction of the harmonic-approximation sequence of the low frequency vibrations of the H_2O dimer.

The replacement of the B97-1 functional by either the OLYP functional or the O3LYP hybrid functional changes the shape and energetic sequence of the lowest

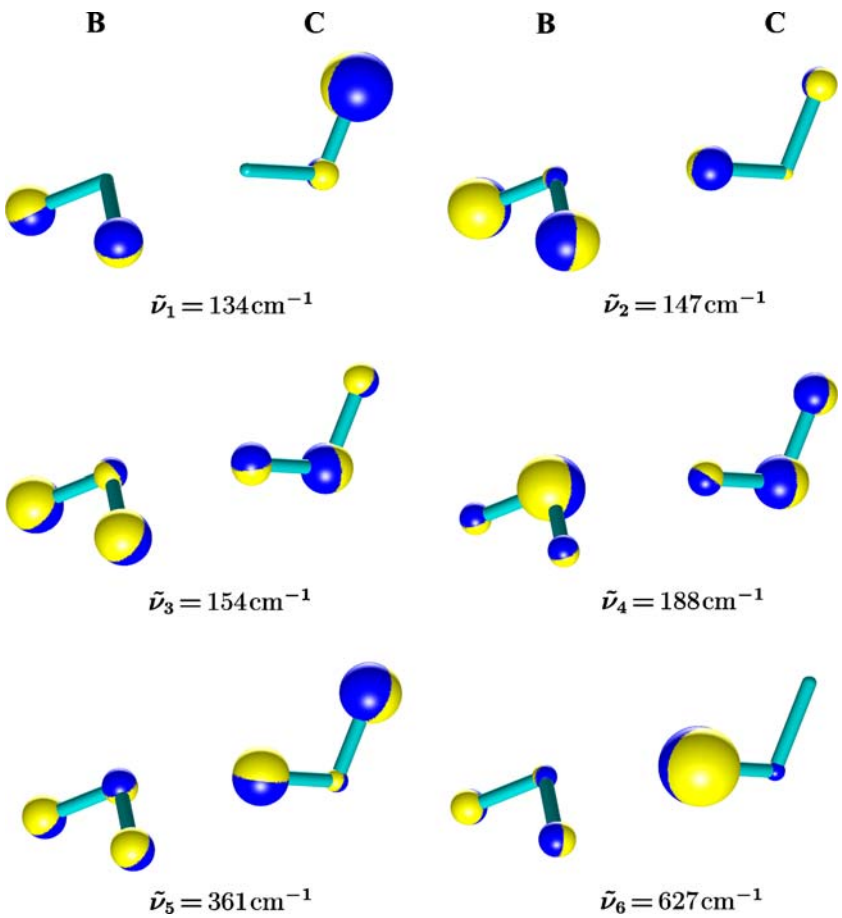

Fig. 4 Vibrational energy distribution of the intermolecular vibrations of the water dimer *A*. The *x*-axis in Table 3 is perpendicular to the dimer's plane of symmetry, *y* points from the center of mass of monomer *B* towards the center of mass of monomer *C*. Computational approach: B97-1/pc-2

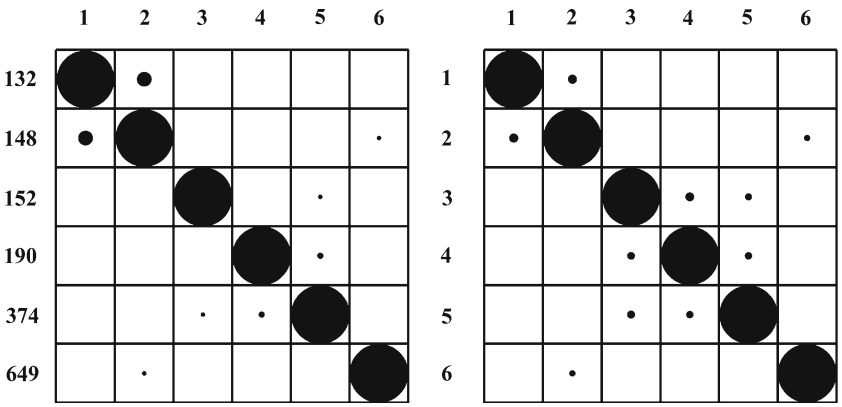

Fig. 5 Overlap of the lowest six vibrations of the H_2O dimer computed with DFT with those computed with CCSD(T)/aug-cc-pVTZ. Going down a column gives the decomposition of a vibration obtained by a DFT procedure into those of the reference method, with the frequencies of the latter indicated at the *far left*. *Left* B97-1/pc-2. *Right* B97-1/rr-pc-2

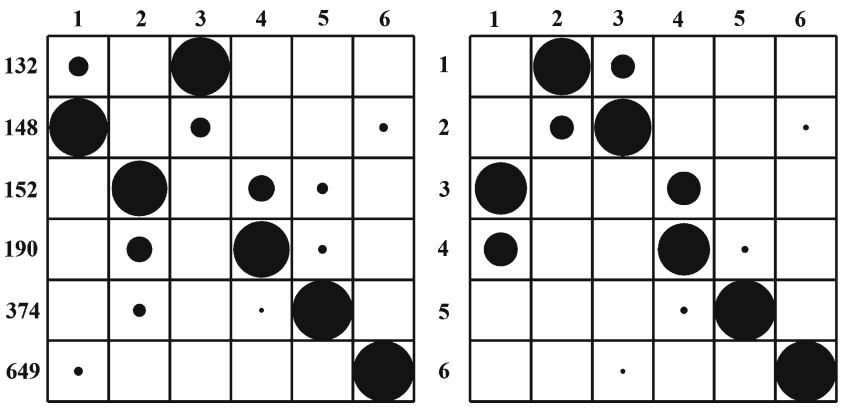

Fig. 6 Overlap of the lowest six vibrations of the H_2O dimer computed with DFT with those computed with CCSD(T)/aug-cc-pVTZ. Going down a column gives the decomposition of a vibration obtained by a DFT procedure into those of the reference method, with the frequencies of the latter indicated at the *far left*. *Left* B97-1/pc-1. *Right* O3LYP/pc-2

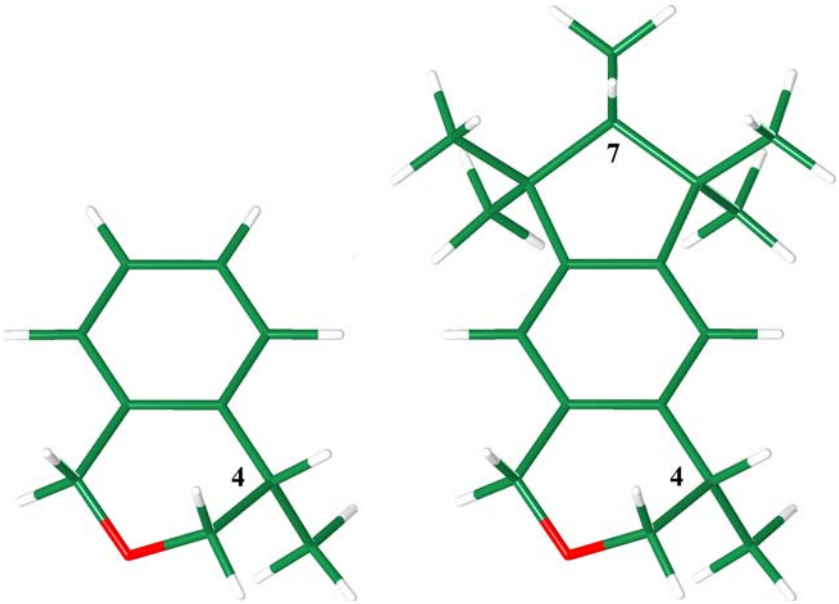

Fig. 7 The pseudo-axial conformers of (4S)-4-methylisochromane (*left*) and (4S,7R)-galaxolide (*right*)

four vibrations. The results for O3LYP/pc-2 are the most favorable ones and included in Fig. 6. One sees that even O3LYP cannot reproduce the CCSD(T) harmonic sequence of the three lowest vibrations, and that, moreover, vibrations 1 and 4 are mixtures of the CCSD(T) vibrations 3 and 4. OLYP and O3LYP are clearly not suited for describing hydrogen bonding.

3.3 Vibrational modes of large molecules

In this section we demonstrate how the vibrational motions of a large molecule, (4S,7R)-galaxolide, can be analyzed in terms of the vibrational motions of two smaller ones with similar structural elements, namely (4S)-4-methylisochromane and o-xylene.

For a molecule like (4S,7R)-galaxolide, the B97-1/pc-2 approach is, at present, not feasible with our modest computational resources. The rr-pc-2 basis [38] set (rr for twice reduced) was born out of the necessity to have a basis set with some of the same qualities as pc-2, but suitable for the DFT calculation of large molecules. It was obtained from pc-2 by removing the *f* functions on the atoms of the first row, and by replacing the two *d* functions by a single one. On hydrogen atoms, the *d* functions were likewise removed, and the two *p* functions were replaced by a single one. The B97-1/rr-pc-2 approach was used throughout this section.

Comparison of (4S,7R)-galaxolide and (4S)-4-methylisochromane. In both of these chiral molecules the methyl group at position 4 can assume either a pseudo-axial or a pseudo-equatorial orientation [16]. The pseudo-axial conformer is slightly favored and is the one considered here. Similarly, in galaxolide, the methyl group at position 7 can assume either a pseudo-axial or a pseudo-equatorial orientation. The energy of the pseudo-axial conformer is higher by 12.7 kJ/mol and so only the pseudo-equatorial form is of importance. The computed structures and the numbering of the atoms of the two molecules are shown in Fig. 7.

The two molecules have far too many vibrational modes for a comprehensive discussion. The 45 nuclei of (4S,7R)-galaxolide lead to 129 vibrational modes, while the 23 nuclei of (4S)-4-methylisochromane yield 63. The largest common fragment of the two molecules has 21 nuclei (Fig. 8). In order to identify similar nuclear motions in a systematic way, all the displacement vectors of these 21 nuclei for 192 vibrations must be compared. This was done by contracting dyads by an automated procedure.

We limit the comparison here to the subsets of the ten vibrations 38–47 (779–946 cm^{-1}) of (4S,7R)-galaxolide and of the ten vibrations 15–24 (727–989 cm^{-1}) of (4S)-4-methylisochromane. This spectral range is part of the fingerprint region where conventional methods for correlating vibrational motions fail to provide useful information.

The first question one may ask is if there are, in the chosen wavenumber range, vibrations which strongly overlap on the largest common fragment MIC (Fig. 8). Figure 9 shows that, while overlap for many vibrations is substantial, it is also far from complete, with the largest values barely exceeding 0.5 (this corresponds to the surface of the largest circular discs in Fig. 9).

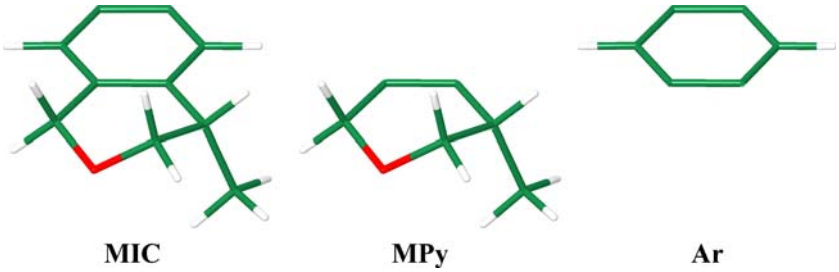

Fig. 8 The fragments on which the vibrations 38–47 of (4S,7R)-galaxolide are compared with the vibrations 15–24 of (4S)-4-methylisochromane. *Left* fragment MIC with the 21 common nuclei of the methylisochromane moiety. *Middle* fragment MPy with the 15 common nuclei of the methylpyrane moiety. *Right* fragment Ar with the 8 common nuclei of the aromatic moiety

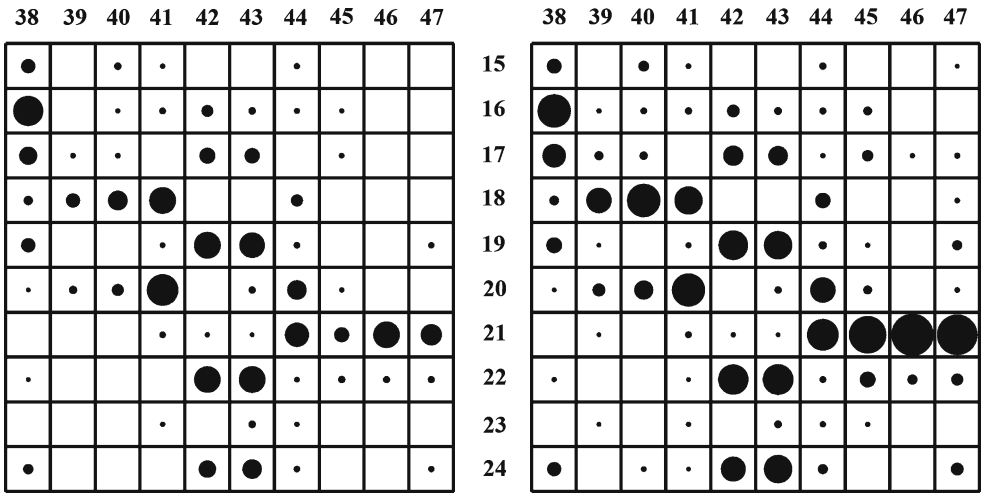

Fig. 9 Representation of overlap (*left*) and similarity (*right*) in graphical form for fragment MIC. The columns correspond to the vibrations of (4S,7S)-galaxolide, and the rows to the vibrations of (4S)-4-methylisochromane. A *circle* with a diameter equal to the *square* which contains it means a value of 1

An absence of strong overlap can be due to the dissimilarity of the shape of the vibrations, or it can be due to a lack of the localization of the vibrations on the fragment one inspects. From the similarity also depicted in Fig. 9 one sees that both aspects are important for the MIC fragment. There is one pair of vibrations for which similarity reaches 0.95, namely 46 for (4S,7R)-galaxolide and 21 for (4S)-4-methylisochromane. A further pair, 47 and 21, comes close, with a value of 0.87. These vibrations are depicted in Fig. 10. For the other vibrations of the chosen sets, similarity is lower.

Reducing the size of a fragment can increase similarity though it will, for vibrations which extend beyond the fragment, reduce overlap. This is born out in Fig. 11 for the methylpyrane moiety MPy.

The pattern of nuclear displacements exhibited by vibration 21 on the MPy moiety of (4S)-4-methylisochromane is particularly persistent. It shows up, with a similarity of 0.7, 0.94, 0.99, and 0.99, in the vibrations 44, 45, 46, and 47, respectively, in (4S,7R)-galaxolide. The characteristic nuclear motions on the MPy fragment are strikingly coupled in (4S,7R)-galaxolide with nuclear motions on the distant pentamethyl-cyclopentane fragment, rather than with vibrations on the neighboring Ar fragment.

The different behavior of overlap and similarity illustrates the fact that the *shape* of nuclear motions is often similar even when the *size* of nuclear motions is not. The directions, and the relative size, of the small excursions on the MPy moiety of (4S,7R)-galaxolide in vibration 47, e.g., agree to 99% with those of the far larger excursions of vibration 21 in (4S)-4-methylisochromane. We may consider such persistent similarity, independent of excursion, the hallmark of a group vibration.

Comparison with o-xylene. As a corollary, we present in Fig. 12 vibration 44 of (4S,7R)-galaxolide and vibration 18 of (4S)-4-methylisochromane. Both vibrations

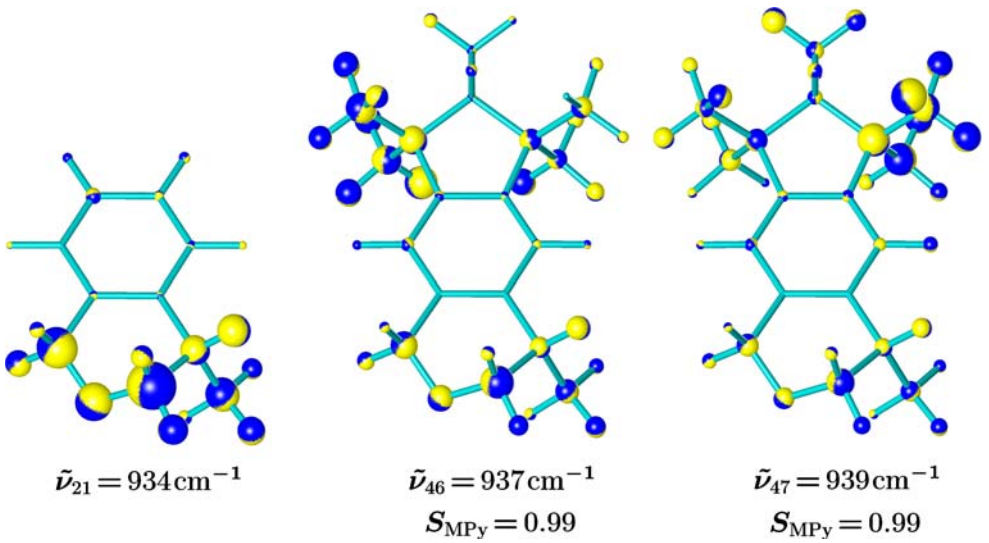

Fig. 10 Examples of vibrations with a high similarity on the MIC moiety due to motion on MPy. S_{MPy}: value of the similarity of the motions of the 13 nuclei of MPy of (4S,7R)-galaxolide and (4S)-4-methylisochromane. Representation: vibrational energy distribution

are distributed over the whole of these molecules. The motions of the eight nuclei of the aromatic moiety Ar are strikingly similar, but not identical, for the two molecules, with similarity reaching 0.63 on Ar—the highest on this fragment for the chosen set of vibrations. Overlap, on the other hand, is negligible, as is already evident from Fig. 9. The motions of the eight nuclei of Ar are closely related to those of a vibration of A'' symmetry of o-xylene shown also in Fig. 12. The similarity of this vibration with the vibrations 18 of (4S)-4-methylisochromane and 44 of (4S,7R)-galaxolide on Ar is 0.7 and 0.68, respectively.

On the pentamethyl-cyclopentane moiety, vibration 44 comes close to transforming according to the A'' representation of the local point group C_s of this fragment. The local mirror planes of the aromatic and of the cyclopentane moiety are both oriented in the same way, and so the coupling of a motion on the fragment Ar with A'' symmetry in o-xylene with an A'' type motion on the cyclopentane fragment is what one expects.

4 Conclusions

It is a recent development that the vibrational modes of large molecules, and of clusters of molecules, if composed mainly of hydrogen and first-row atoms, can be reliably computed. The availability of such data has opened the need for understanding them. We demonstrate in this article that it is possible to comprehend large-scale computed nuclear motions, encompassing an ensemble of several dozen nuclei, through a decomposition into the vibrational, rotational, and translational motions of characteristic subunits. The judicious choice of subunits can bypass many of the limitations of the decomposition into the more traditional valence coordinates. Through the availability of a program with a convenient graphical interface [31], we expect the approach to become a standard method for analyzing the vibrations of large molecules.

The proposed decomposition is meaningful only if computed large-scale nuclear motions are physically meaningful. One might therefore ask, how do we know that this is so? The conclusive evidence comes from the agreement of computed and measured vibrational spectra. Raman optical activity and vibrational circular dichroism spectra, in particular, are highly sensitive not just to the energy of the vibrational modes, but even more so to their shape. The conclusive demonstration that DFT can yield vibrational modes which lead to good agreement between computed and measured VCD [44] and ROA [14,15] spectra of large, non-symmetric molecules must be considered a major advance in the field of molecular mechanics.

The decomposition of vibrational modes as outlined here can yield further important arguments in support of ab initio computed vibrational shapes. The limited material we present suggests that extended vibrational motions of large molecules are quite logically composed of characteristic motions of subunits. This is demonstrated by the comparison of some of the modes of (4S,7R)-galaxolide, (4S)-4-methylisochromane, and o-xylene. The persistence of nuclear motions on symmetric as well as non-symmetric fragments of such

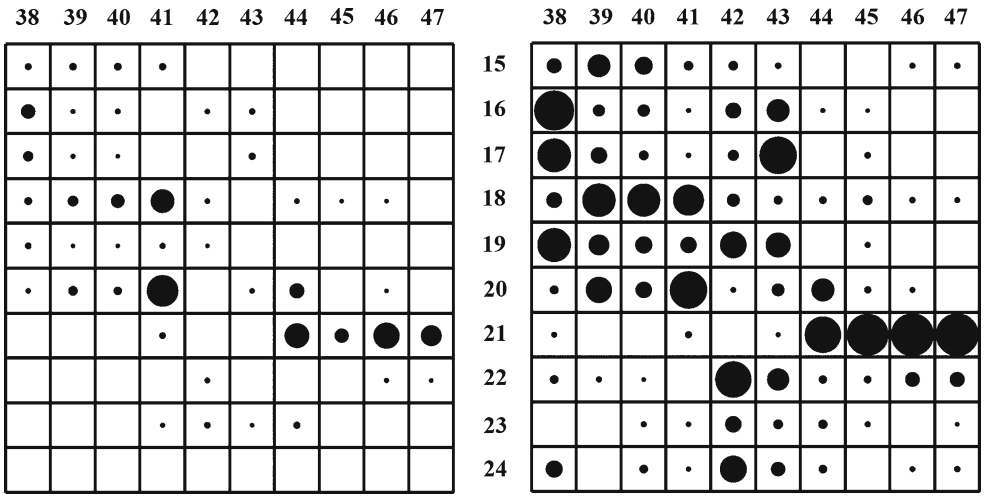

Fig. 11 Representation of overlap (*left*) and similarity (*right*) in graphical form for fragment MPy. The columns correspond to the vibrations of (4S,7S)-galaxolide, and the rows to the vibrations of (4S)-4-methylisochromane. A *circle* with a diameter equal to the *square* which contains it means a value of 1

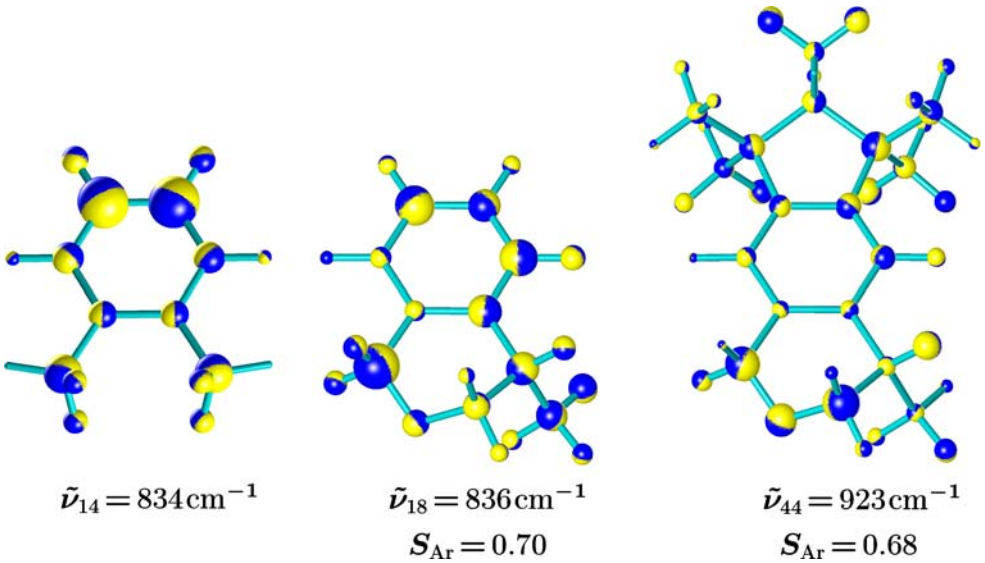

Fig. 12 Similar vibrations on the aromatic fragment Ar. S_{Ar}: value of the similarity on Ar of (4S)-4-methylisochromane (*middle*) and (4S,7R)-galaxolide (*right*) with the eclipsed rotamer of o-xylene (*left*). Representation: vibrational energy distribution

molecules is astounding, with some of the more obvious resemblances already recognized [16] ahead of the availability of the present decomposition of vibrational modes.

A decisive aspect of the method we propose is, of course, that it allows us to quantify the notions of overlap and similarity. The mere visual tracking down of resemblances of nuclear motions does not discover similarity as defined here, but overlap. This is at the root of the problem of identifying, by visual inspection alone, highly similar but small motions on extended vibrational chromophores, even though they seem to be a common occurrence. The similarity on the aromatic fragment of mode 44 of (4S,7R)-galaxolide with mode 14 of o-xylene is a point in case.

The quantitative assessment of the mixing of the vibrations of individual subunits, by their being part of a larger system, is an important but so far unexplored aspect of vibrational optical activity. We demonstrate the disentanglement of mingled vibrational modes for a simple non-chiral system, the dimer of formic acid. In this example, hydrogen bonding in the dimer mixes

selectively, and unexpectedly, some of the monomers' bending vibrations. In some chiral carboxylic acids we have studied, this is at the origin of large and characteristic vibrational optical activity.

The influence of external perturbations and of anharmonicity are not studied here. From the demonstrated sensitivity of the method for identifying small changes in computed intermolecular potentials, such as those produced by differing computational approaches for the H_2O dimer, it is evident, however, that the approach is well suited for quantifying changes due to solvent interactions and anharmonic potentials. Both perturbations are expected to influence the shape of nuclear motions, and both are therefore of practical interest in a future refinement of the theoretical treatment of vibrational optical activity.

Note added in proof: Since submitting our manuscript, the ViPA (vibrational projection analysis) method [Grafton AK, Wheeler RA (1998) J Comp Chem 19:1663] has been brought to our attention. It uses, similarly to much earlier work [Duschinsky F (1937) Acta Physicochim URSS 7:551] of which we were likewise not aware, the scalar product for comparing vibrational motions. The Eckart-Sayvetz conditions are not taken into account in the ViPA method. As translations, rotations, and vibrations of individual units are not separately considered it cannot, in contrast to the method described here, compare such motions on distinct fragments of different molecules or clusters. The lack of a standardized way of aligning entities would also appear to render numerical results geometry dependent.

Acknowledgments The authors are grateful to Prof. Frank Jensen for providing helpful details on his basis sets. The computations were done on the Opteron cluster of the University of Fribourg. The project was supported by the Swiss National Science Foundation under grant number 200020-103750.

References

1. Sverdlov LM, Kovner MA, Krainov EP (1974) Vibrational spectra of polyatomic molecules. Halsted, New York
2. Holzwarth G, Hsu EC, Mosher HS, Faulkaner TR, Moscowitz A (1974) J Am Chem Soc 96:251
3. Nafie LA, Cheng JC, Stephens PJ (1975) J Am Chem Soc 97:3842
4. Nafie LA, Keiderling TA, Stephens PJ (1976) J Am Chem Soc 98:2715
5. Barron LD, Bogaard MP, Buckingham AD (1973) J Am Chem Soc 95:603
6. Barron LD, Bogaard MP, Buckingham AD (1973) Nature 241:113
7. Hug W, Kint S, Bailey GF, Scherer JR (1975) J Am Chem Soc 97:5589
8. Herzberg G (1945) Molecular structure and molecular spectra. II. Infrared and Raman spectra of polyatomic molecules. van Nostrand, New York
9. Wilson EB, Decius JC, Cross PC (1955) Molecular vibrations. Dover, New York
10. Fogarasi G, Pulay P (1985) Vib Spectra Struct 14:125–219
11. Dollish FR, Fateley WG, Bentley FF (1974) Characteristic Raman frequencies of organic compounds. Wiley, New York
12. Colthup NB, Daly LH, Wiberly SE (1975) Infrared and Raman spectroscopy. Academic, New York
13. Ashvar CS, Devlin FJ, Stephens PJ, Bak KL, Eggimann T, Wieser H (1998) J Phys Chem A 102:6842–6857
14. Hug W, Zuber G, de Meijere A, Khlebnikov AF, Hansen H-J (2001) Helv Chim Acta 84:1
15. Ruud K, Helgaker T, Bouř P (2002) J Phys Chem A 106:7448
16. Zuber G, Hug W (2004) Helv Chim Acta 87:2208
17. Jalkanen KJ, Nieminen RM, Frimand K, Bohr J, Bohr H, Wade RC, Tajkhorshid E, Suhai S (2001) Chem Phys 65:125
18. Jalkanen KJ, Nieminen RM, Knapp-Mohammady M, Suhai S (2003) Int J Quant Chem 92:239
19. Stephens PJ, Devlin FJ, Chabalowsky CF, Frisch MJ (1994) J Phys Chem 98:11623
20. Stephens PJ, Devlin FJ, Ashvar CS, Chabalowsky CF, Frisch MJ (1994) Farad Discuss 99:103–119
21. Hug W (2001) Chem Phys 264:53
22. Califano S (1976) Vibrational States. Wiley, New York
23. Melnik DG, Gopalakrishnan S, Miller TA (2003) J Chem Phys 118:3589
24. Cuony B, Hug W (1981) Chem Phys Lett 84:131
25. Goldstein H (1980) Classical mechanics. Addison-Wesley, Reading
26. Rosenfeld L (1965) Theory of electrons. Dover, New York
27. Kabsch W (1976) Acta Cryst A32:922–923
28. Kabsch W (1978) Acta Cryst A34:827–828
29. Heisterberg DJ (1990) A program to superimpose atoms of two molecules by the quaternion method. http://www.ccl.net/cca/software/SOURCES/C/quaternion-mol-fit/quatfit.c
30. Kneller GR (1991) Mol Simul 7:113–119
31. Fedorovsky M (2006) PyVib2, a program for analyzing vibrational motion and vibrational spectra, 2006. To be published under the general public licence.
32. Becke AD (1997) J Chem Phys 107:8554
33. Hamprecht FA, Cohen AJ, Tozer DJ, Handy NC (1998) J Chem Phys 109:6264
34. Jensen F (2001) J Chem Phys 115:9113–9125
35. Jensen F (2002a) J Chem Phys 116:7372–7379
36. Jensen F (2002b) J Chem Phys 117:9234–9240
37. Frisch MJ, Trucks GW, Schlegel HB, Scuseria GE, Robb MA, Cheeseman JR, Montgomery JA Jr, Vreven T, Kudin KN, Burant JC, Millam JM, Iyengar SS, Tomasi J, Barone V, Mennucci B, Cossi M, Scalmani G, Rega N, Petersson GA, Nakatsuji H, Hada M, Ehara M, Toyota K, Fukuda R, Hasegawa J, Ishida M, Nakajima T, Honda Y, Kitao O, Nakai H, Klene M, Li X, Knox JE, Hratchian HP, Cross JB, Bakken V, Adamo C, Jaramillo J, Gomperts R, Stratmann RE, Yazyev O, Austin AJ, Cammi R, Pomelli C, Ochterski JW, Ayala PY, Morokuma K, Voth GA, Salvador P, Dannenberg JJ, Zakrzewski VG, Dapprich S, Daniels AD, Strain MC, Farkas O, Malick DK, Rabuck AD, Raghavachari K, Foresman JB, Ortiz JV, Cui Q, Baboul AG, Clifford S, Cioslowski J, Stefanov BB, Liu G, Liashenko A, Piskorz P, Komaromi I, Martin RL, Fox DJ, xKeith DJ, Al-Laham MA, Peng CY, Nanayakkara A, Challacombe M, Gill PMW, Johnson B, Chen W, Wong MW, Gonzalez C, Pople JA (2004) Gaussian 03, Revision C.01. Gaussian Inc., Wallingford

38. Hug W, Fedorovsky M (2006) To be published
39. Hug W, Haesler J (2005) Int J Quant Chem 104:695–715
40. Handy NC, Cohen AJ (2001) Mol Phys 99:403
41. Hoe W-M, Cohen AJ, Handy NC Chem Phys Lett 341:319
42. Kendall RA, Dunning TH Jr (1992) J Chem Phys 96:6796–6806
43. Stanton JF, Gauss J, Watts JD, Nooijen M, Oliphant N, Perera SA, Szalay PG, Lauderdale WJ, Kucharski SA, Gwaltney SR, Beck S, Balkova A, Bernholdt DE, Baeck KK, Rozyczko P, Sekino H, Hober C, Bartlett RJ (2005) ACESII, Advanced Concepts in Electronic Structure, v.2.4.0-stable
44. Cheeseman PJ, Frisch MJ, Devlin FJ, Stephens PJ (1996) J Chem Phys Lett 252:211